Heat-Shrinking Spherical and Columnar Supramolecular Dendrimers: Their Interconversion and Dependence of Their Shape on Molecular Taper Angle

Goran Ungar,*[a] Virgil Percec,*[b] Marian N. Holerca,[b] Gary Johansson,[b] and James A. Heck[b]

Abstract: Synthesis and modes of self-assembly are described for the tapered monodendritic molecules 3,4,5-nG$_i$-X of generation $i = 1$, 2, 3 (see structures below) that contain multiple $(CH_2)_nH$ alkyl chains on their periphery ($n = 12$, 14, 16) and a polar group X at the apex (X = COOH, COONa, COOCs, $CO(OCH_2CH_2)_3OH$). These monodendrons self-assemble into supramolecular cylindrical or spherical dendrimers, which in turn self-organise into *p6mm* columnar or $Pm\bar{3}n$ cubic thermotropic liquid crystals, respectively. The two principal ways of affecting the self-assembly of these compounds by means of their molecular architecture are: a) by changing the width of the wide (aliphatic) end, and b) by changing the volume at the apex. In the present work a) is controlled through temperature (conformational disorder) and b) is controlled by changing the generation number i or the size of X, for example, through the choice of metal cation. The single most important geometric parameter of these dendritic building blocks is the molecular solid angle (taper angle) α; a high α leads to spherical and a low α to cylindrical supramolecular dendrimers. Furthermore, α also determines the equilibrium size of the supramolecular objects; a larger α results in a smaller diameter. The unusually strong negative thermal expansion coefficient of the cubic and columnar lattice is attributed to the excess of the increasingly highly tapered molecules being rejected from their parent aggregates and reassembling as new ones. Increasing α is also considered to be responsible for the observed thermotropic columnar–cubic transition.

Keywords: cubic · dendrimers · liquid crystals · supramolecular chemistry · X-ray diffraction

Introduction

It is well known that disk-like molecules form columnar liquid crystals, in which the disks stack up and create infinite columns. The columns in turn pack laterally in a two-dimensional, mostly hexagonal lattice.[1] Columnar liquid crystals can also evolve through self-assembly of taper-shaped molecules whose wide end is usually made up of two or three flexible aliphatic chains.[2, 3] Self-assembly of such tapered molecules into columns can be visualised as packing of slices to form a "pizza" and stacking of "pizzas" on top of one another (Scheme 1a). We have recently demonstrated how the mode of self-assembly can be changed from columnar to spherical by linking tapered first-generation monodendrons together into higher generation monodendrons (Scheme 1b).[4]

In this publication, we demonstrate the link between the molecular geometry of the monodendritic building block and the shape and size of the resulting supramolecular dendrimer. Furthermore, we show how the diameter of the spherical and columnar supramolecular dendrimers decreases with increasing temperature and, related to this, how the supramolecular column–sphere transition can be induced thermally. The systems described here can in some respects be regarded as simple synthetic models of complex biological self-assembled structures, such as the cylindrical tobacco mosaic virus and spherical viruses.[5]

[a] Dr. G. Ungar
Department of Engineering Materials
and Centre
for Molecular Materials
University of Sheffield, Sheffield S1 3JD (UK)
Fax: (+44) 114-222-5943
E-mail: g.ungar@sheffield.ac.uk

[b] Prof. V. Percec, M. N. Holerca, Dr. G. Johansson, Dr. J. A. Heck
Roy & Diana Vagelos Laboratories
Department of Chemistry, University of Pennsylvania, Philadelphia
PA 19104-6323 (USA)
E-mail: percec@sas.upenn.edu

Results and Discussion

Supramolecular dendrimers from taper-shaped monodendrons: Simple examples of tapered monodendrons that self-assemble into columns are compounds designated as 3,4,5-nG$_1$-X (see structures below), where $R = (CH_2)_nH$ (n of $(CH_2)_n$ is identical to n in 3,4,5-nG$_1$-X) and X is an ionophore (for example, a crown-ether salt complex or an oligo(ethyleneoxide) salt complex),[3] a hydrogen bonding group,[6]

0947-6539/00/0607-1258 $ 17.50+.50/0 *Chem. Eur. J.* **2000**, *6*, No. 7

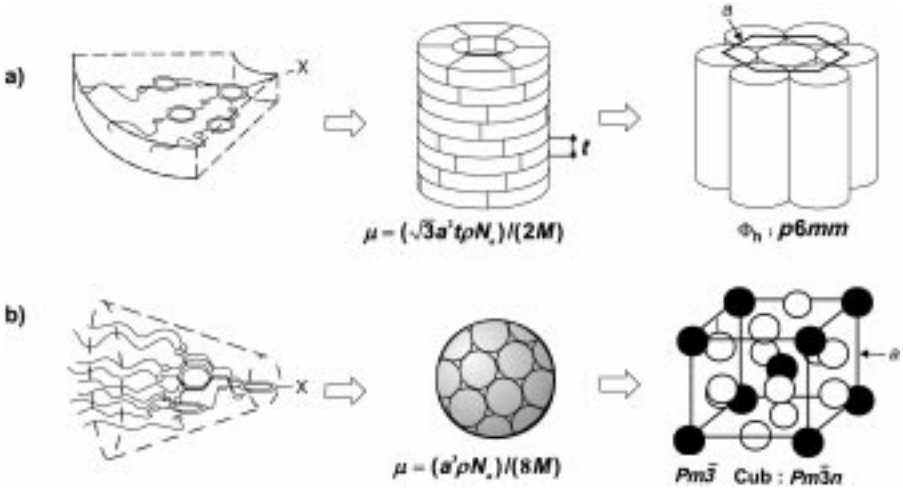

Scheme 1. a) Schematic representation of the self-assembly of flat tapered monodendrons into a supramolecular cylindrical dendrimer and of the self-organisation of such cylinders into a *p6mm* hexagonal columnar (ϕ_h) liquid crystal; b) self-assembly of conical monodendrons into a supramolecular spherical dendrimer and of the self-organisation of the latter into a $Pm\bar{3}n$ cubic (Cub) liquid crystal. (μ = average number of monodendrons in a disk or sphere, a = lattice parameter, t = thickness of a disk, M = molecular weight of monodendron, ρ = density, N_a = Avogadro's number). X = endo receptor or functional group.

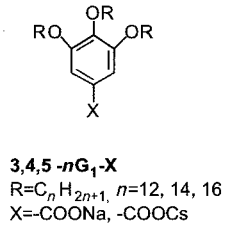

3,4,5 -*n*G$_1$-X
R=C$_n$H$_{2n+1}$, *n*=12, 14, 16
X=-COONa, -COOCs

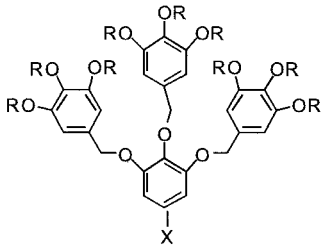

(3,4,5)^2-12G$_2$-X
R=-C$_{12}$H$_{25}$
X=-COOH or
X=-CO(OCH$_2$CH$_2$)$_3$OH

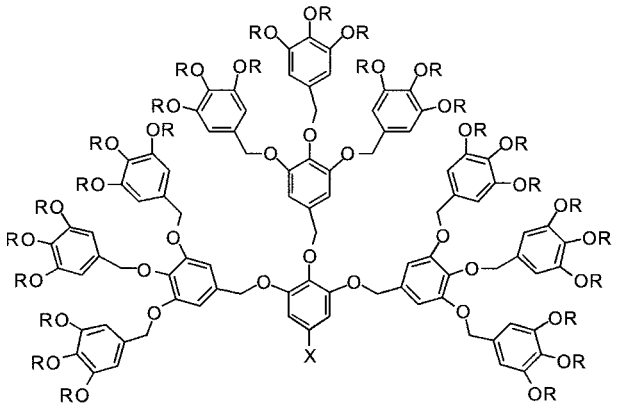

(3,4,5)^3-12G$_3$-X
R=-C$_{12}$H$_{25}$
X=-COOH

or a covalent linkage to a polymer backbone.[3c, 3e, 7] The thermotropic columnar liquid crystals formed from these compounds are characterised by periodic density fluctuations in two dimensions. The high-density regions are made up predominantly of the aromatic molecular cores self-assembled into rods of infinite length.[6] The low-density matrix consists of tethered aliphatic chains. Such structures can provide templates, for example, for ionic channel arrays.[8]

The second, third and fourth generation dendrons from the same series as 3,4,5-12G$_1$-X, that is, (3,4,5)^i-12G$_i$-X where i = 2, 3 and 4, self-assemble into spherical supramolecular dendrimers which, in turn, self-organise in a thermotropic cubic lattice (Scheme 1b).[4] This cubic phase is stable in a comparatively wide-temperature range (Table 1). The chemical structures of the first three generations of monodendrons from this series are shown in the structures illustrated. All these molecules consist of a predominantly aromatic dendritic core end-capped with R = -(CH)$_{12}$H chains and they contain various functionalities (X) at their core.

Molecular modelling shows that, while a 3,4,5-12G$_1$-X molecule may fit into a flat disk segment that allows stacking into infinite columns, this is not possible with higher generations of (3,4,5)^i-12G$_i$-X as a result of the steric overcrowding of the large number of terminal chains.[4] Thus, such monodendrons can no longer be described as slice-shaped, but rather as pyramid- or cone-shaped (Scheme 1 and Figure 1a,b). Therefore, instead of forming infinite columns, such cones self-assemble into closed isolated spherical objects, which in turn pack in a periodic cubic lattice (Scheme 1b, Figure 1c–e).

Monodomain and powder X-ray diffraction,[4a] supported by transmission electron microscopy,[3k] has shown that the space group of the cubic phase is $Pm\bar{3}n$ (Q^{223}). Based on measured diffraction intensities, electron density distribution within the unit cell was computed by Fourier synthesis for the series of carboxylic acids denoted here as (3,4,5)^i-12G$_i$-COOH, with i = 2, 3 and 4. Two- and three-dimensional (isosurface) maps[4a, 3m] have shown eight spherical or nearly spherical regions of highest electron density per unit cell. These represent the centres of the self-assembled supramolecular dendrimers. In Figure 2, they are shown schematically as the smaller spheres. Each of these represents the clustered aromatic regions of a number of monodendron molecules. The outer spheres in Figure 2 that merge with one another represent schematically the outer spheres shown in Figure 1c; the volume between the inner and the outer sphere is about 80% of the total, which is occupied predominantly by the aliphatic chains. Since in reality aliphatic chains provide a space-filling continuum, the outer spheres in Figures 1c and 2 are in fact approximations of the two dodecahedra and six tetrakaidecahedra, which divide exactly the full unit cell volume.[9] A similar cubic phase of the micellar type has previously been found in some lyotropic lipid–water systems,

Table 1. Transition temperatures and corresponding enthalpy changes of $(3,4,5)^i$-nG_i-X monodendrons. Data for entries 6–9 are from [4a].

	Monodendron	Transition temperatures [°C] and corresponding enthalpy changes [kcal mol^{-1}]	
		Heating (first and second)	Cooling
1	3,4,5-12G_1-COOH	*k* 60 (14.9) *i* *k* 59 (14.3) *i*	*i* 33 (14.1) *k*
2	3,4,5-12G_1-COONa	*k* 48 (6.27) ϕ_h 96 (5.30) ϕ_h 119 (0.5) Cu *k* 3 (2.9) ϕ_h 96 (0.7) ϕ_h 119 (0.9) Cu	Cu 100 (0.9) ϕ_h −6 (2.4) *k*
3	3,4,5-12G_1-COOCs	*k* 66 (12.5) ϕ_h 119 (broad) (1.7) ϕ_h 170 (0.5) Cu *k* 3 (2.9) *k* 51 (0.4) ϕ_h 172 (0.6) Cu	Cu 162 (0.4) ϕ_h 41 (0.6) *k* −9 (2.5) *k*
4	3,4,5-14G_1-COOCs	*k* 67 (17.7) ϕ_h 143 (1.6) Cu *k* 39 (6.8) ϕ_h 154 (0.8) Cu	Cu 145 (0.6) ϕ_h 21 (6.7) *k*
5	3,4,5-16G_1-COOCs	*k* 75 (30.0) ϕ_h 132 (0.7) Cu 150 (0.6) Cu *k* 56 (12.6) ϕ_h 146 (0.8) Cu	Cu 137 (0.7) ϕ_h 39 (11.5) *k*
6	$(3,4,5)^2$-12G_2-COOH	*k* 85 (25.6) Cu 119 (1.3) *i* *k* −9 (5.6) *k* 43 (−19.5) *k* 83 (24.3) Cu 117 (1.0) *i*	*i* 111 (0.9) Cu −15 (8.7) *k*
7	$(3,4,5)^2$-12G_2-CO$(OCH_2CH_2)_3$OH	*k* 56 (37.9) *i* *k* 56 (28.6) Cub 59 (0.3) *i*	*i* 44 (0.3) Cub 1 (18) *k*
8	$(3,4,5)^3$-12G_3-COOH	*k* −15 (31.5) Cu 140 (1.6) *i* *k* −12 (29.7) Cu 139 (1.2) *i*	*i* 127 (1.2) Cu −17 (31.0) *k*
9	$(3,4,5)^4$-12G_4-COOH	*k* −14 (83.3) Cu 85 *i* *k* −12 (105.9) Cu 85 *i*	*i* 72 Cu −18 (89.4) *k*

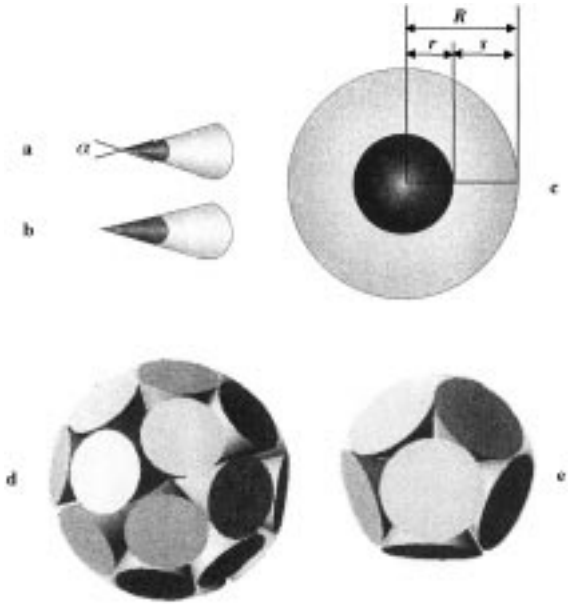

Figure 1. a) Schematic representation of a cone-shaped $(3,4,5)^i$-nG_i-X monodendron fragment with the aromatic rings toward the apex (dark) and the aliphatic chains (light) distributed at the broad end (α is the molecular solid angle); b) same representation for a smaller α due to a larger aromatic volume; c) self-assembled spherical supramolecular dendrimer with an aromatic core of radius *r* and an aliphatic sheath of thickness *s*; d) and e) supramolecular dendrimers self-assembled from long, narrow and short, wide monodendrons, respectively.

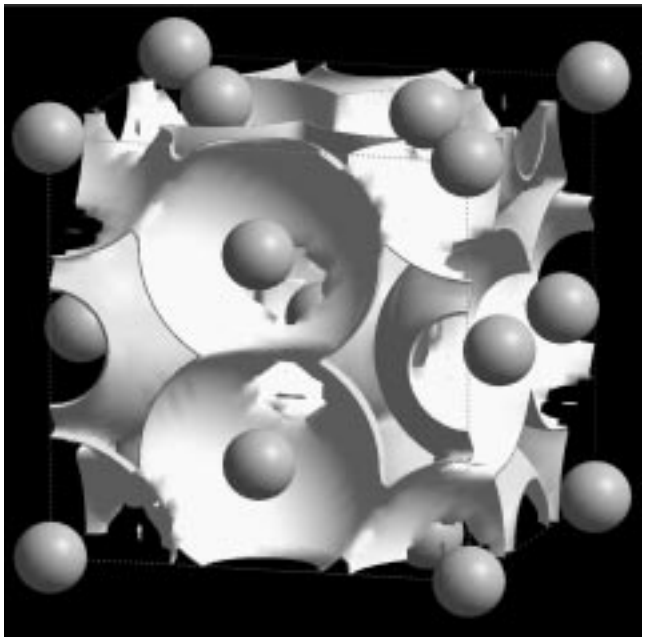

Figure 2. Packing of the schematic spherical supramolecular dendrimers (Figure 1c) on the $Pm\bar{3}n$ cubic lattice. Small spheres represent aromatic regions. The overlapping outer spheres represent aliphatic regions, which, in reality, form a continuum.

although some controversy remains about the exact micellar shape.[10]

The side length of the cubic unit cell is in the 6–9 nm range and each unit cell contains of the order of a hundred molecules or molecular residues of $(3,4,5)^2$-12G_2-COOH (Table 2). In our cubic liquid crystal, the spherical object or aggregate is regarded as a supramolecular dendrimer.[4a] Since the structure is a liquid crystal, individual molecules have no preferred position in the cell and there is no Bragg diffraction in the wide-angle region. Regarding the disordered melt that exists at temperatures above the range of the cubic phase, there is strong diffuse scattering close to the position of the most prominent cubic reflections. This indicates that similar spherical clusters or supramolecular objects persist into the melt proper, but with only a short-range stacking order.

Molecular taper angle and the size of spherical supramolecular dendrimers: It is instructive to consider the variation in the number of molecules per sphere for different monodendritic species in Table 2.[11] Surprisingly, while there are 21 monodendrons of $(3,4,5)^2$-12G_2-CO$(OCH_2CH_2)_3$OH in a

0947-6539/00/0607-1260 $ 17.50+.50/0 *Chem. Eur. J.* **2000**, *6*, No. 7

Table 2. Structural characterisation of the $Pm\bar{3}n$ cubic phase obtained from various $(3,4,5)^i$-nG$_i$-X monodendrons.

		density $\rho_{20\,^\circ C}$ [g cm^{-3}]	f[a] [%]	a[b] [nm] [$\pm$0.04]	number of molecules per unit cell	μ[c]	number of 3,4,5-G$_1$ monodendron fragment per supramolecular sphere
1	3,4,5-12G$_1$-COONa	1.03	15.8	6.38	230	28	28
2	3,4,5-12G$_1$-COOCs	1.02	17.5	6.80[d]	273	34	34
3	$(3,4,5)^2$-12G$_2$-COOH	0.99	18.0	6.83	92	12	35
4	$(3,4,5)^3$-12G$_3$-COOH	0.99	19.0	7.92	47	6	54
5	$(3,4,5)^2$-12G$_2$-CO(OCH$_2$CH$_2$)$_3$OH	1.01	22.4	8.35	167	21	63
6	3,4,5-12G$_1$-COOCs	1.02	17.5	6.80[d]	273	34	34
7	3,4,5-14G$_1$-COOCs	1.03	15.4	7.02[d]	264	33	33
8	3,4,5-16G$_1$-COOCs	1.03	13.7	7.33[d]	269	34	34

[a] f = aromatic volume fraction from molecular model, including polar groups and cations. [b] a = cubic lattice parameter. [c] μ = number of monodendrons per supramolecular sphere. [d] Obtained at 168 °C.

supramolecular sphere, there are only 12 monodendrons on average in a supramolecular dendrimer generated from $(3,4,5)^2$-12G$_2$-COOH. This is the main reason for the larger cell volume of $(3,4,5)^2$-12G$_2$-CO(OCH$_2$CH$_2$)$_3$OH (by 83%) compared with that of $(3,4,5)^2$-12G$_2$-COOH ($(8.35/6.83)^3 = 1.83$, see Table 2). Our proposed explanation for the increased number of molecules per sphere is illustrated in Figures 3b and d, which represent schematically, in two dimensions, the spheres of $(3,4,5)^2$-12G$_2$-COOH and $(3,4,5)^2$-12G$_2$-CO(OCH$_2$CH$_2$)$_3$OH. The overall taper, or solid angle of a $(3,4,5)^2$-12G$_2$-CO(OCH$_2$CH$_2$)$_3$OH monodendron is less than that of a $(3,4,5)^2$-12G$_2$-COOH monodendron because the distance between the broad end and the thin end (apex) of the molecule is extended by the inclusion of the tri(ethyleneoxide) chain (part of the shaded circle in Figure 3d). Therefore, a larger number (μ) of $(3,4,5)^2$-12G$_2$-CO(OCH$_2$CH$_2$)$_3$OH monodendron molecules is required to complete a sphere. In other words, if α is the solid angle of the wedge-shaped molecule, then ideally Equation (1) will apply.

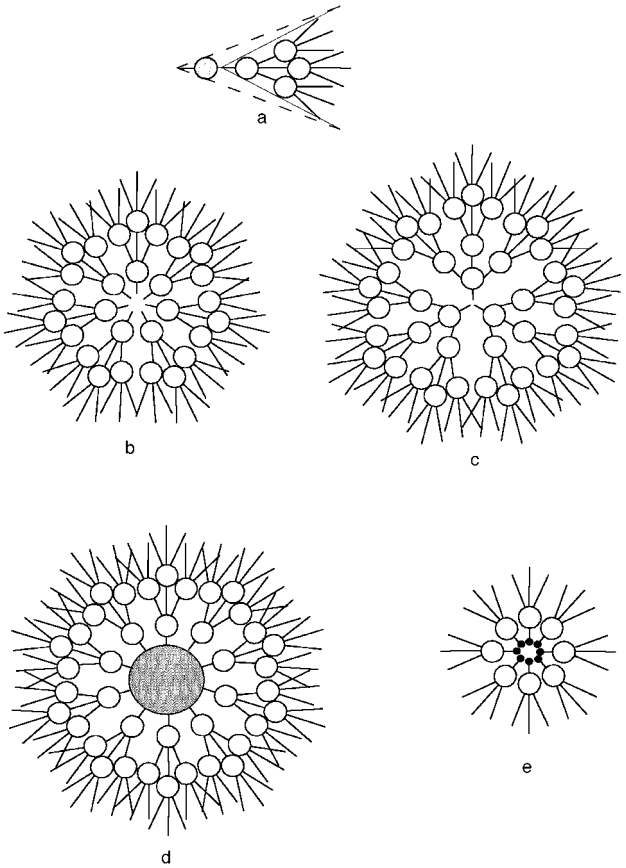

Figure 3. Schematic representation of $(3,4,5)^i$-12G$_i$-X monodendrons: a) a fragment of a $(3,4,5)^3$-12G$_3$-X monodendron with the fragment solid angle α (dashed lines). The larger solid angle of an isolated $(3,4,5)^2$-12G$_2$-X molecule is indicated by thin solid lines; b) a spherical supramolecular dendrimer obtained from $(3,4,5)^2$-12G$_2$-X; c) the increase in the number of $(3,4,5)^2$-12G$_2$ monodendrons per sphere self-assembled from $(3,4,5)^3$-12G$_3$-X; d) a sphere self-assembled from $(3,4,5)^2$-12G$_2$-CO(OCH$_2$CH$_2$)$_3$OH (the grey circle represents the ethyleneoxide core); e) a sphere self-assembled from 3,4,5-nG$_1$-COOM (the black dots represent cations).

$$\mu = \frac{4\pi}{\alpha} \quad (1)$$

At first sight, it may be similarly surprising to find that on moving from $(3,4,5)^2$-12G$_2$-X to $(3,4,5)^3$-12G$_3$-X the unit cell volume increases by a factor of 1.56 [$(7.92/6.83)^3$] and the number of monodendron molecules per sphere, μ, decreases only to one half (from 12 to 6) rather than to one third (that is, to 4) (Table 2). A $(3,4,5)^3$-12G$_3$-X monodendron consists essentially of three $(3,4,5)^2$-12G$_2$ residues (fragments) plus only one additional tri(methyleneoxy)phenyl group (Figure 3c and Scheme 1) and it has a van der Waals volume 3.04 times that of three $(3,4,5)^2$-12G$_2$-X molecules. One might therefore expect that the number of molecules per sphere for $(3,4,5)^2$-12G$_2$-X and $(3,4,5)^3$-12G$_3$-X would be in the ratio 3:1 and not 2:1 as observed. The discrepancy can again be explained by the difference in molecular taper of a $(3,4,5)^2$-12G$_2$-X unit. The additional benzene ring reduces the solid angle α subtended by one third of the $(3,4,5)^3$-12G$_3$-X dendron compared with that subtended by one free molecule of $(3,4,5)^2$-12G$_2$-X (Figure 3a). Consequently, since α is smaller for a $(3,4,5)^2$-12G$_2$-X residue in $(3,4,5)^3$-12G$_3$-X than in the free $(3,4,5)^2$-12G$_2$-X molecule, the number of such residues per sphere is higher in the former. If this number was as high in the latter case as in the former, that is, 18, this would have left a vacancy in the centre of a $(3,4,5)^2$-12G$_2$-X based sphere. In the case of $(3,4,5)^3$-12G$_3$-X, this vacancy is filled by the extra tri(methyleneoxy)phenyl groups, while in the case of $(3,4,5)^2$-12G$_2$-CO(OCH$_2$CH$_2$)$_3$OH it is filled by the tri(ethyleneoxide) chains (Figure 3d). Thus a relatively minor addition of matter at the apex of the residue leads to a pronounced increase in the number of $(3,4,5)^2$-12G$_2$ residues per sphere and hence in a large increase in the volume of a sphere and of the unit cell as a whole.

In view of the effect of the monodendron generation number on the sphere size, it would be of interest to include the 3,4,5-12G_1-X dendrons in this study. As it happens, 3,4,5-*n*G_1-COOH compounds do not show any liquid crystal phase, either columnar or cubic (Table 1). However, salts of such acids, 3,4,5-*n*G_1-COOM (where M is an alkali metal), are liquid crystalline over a wide temperature range. A comprehensive account of their phase behaviour will be given elsewhere. Here we only present a few examples, which allow us to draw more general conclusions about the role of the taper angle, α, on phase type and aggregate size.

At high temperatures, most 3,4,5-*n*G_1-COOM salts with M^+ larger than Li^+ display the $Pm\bar{3}n$ cubic phase. It is interesting to compare two different salts with the same alkyl chain length but with cations of different diameters, 3,4,5-*n*G_1-COOCs and 3,4,5-*n*G_1-COONa. Since the cations are located near the centre of the sphere (Figure 3e), although the change from Na^+ to Cs^+ increases the total volume of a 3,4,5-*n*G_1-COOM pair by only 1.7%, the total volume of the sphere, $a^3/8$, increases by 21% [$(6.80/6.38)^3 = 1.21$, Table 2]. This amplifying effect on sphere size, through incorporation of additional molecules to compensate for reduced effective taper, parallels the effect of incorporation of tri(ethyleneoxide) groups in $(3,4,5)^2$-12G_2-CO$(OCH_2CH_2)_3$OH or of the additional tri(methyleneoxy)phenyl group at the apex of a higher generation monodendron.

In Table 2, geometric parameters of the $Pm\bar{3}n$ phase are summarised for selected salts, alongside those for higher generation dendrons. In the top part of Table 2 (entries 1–5), compounds with dodecyloxy chains are listed in the ascending order of "aromatic volume fraction", *f*, that is, that fraction of the van der Waals volume occupied by all but the alkyl part of the molecule. It is instructive to note the good correlation between the value of *f* and the cubic lattice parameter *a* and, accordingly, the volume per sphere. The number of molecules per unit cell is calculated using known densities.[4] To assist comparison between different compounds, the last column in Table 2 lists the number of 3,4,5-12G_1 monodendron fragments per supramolecular sphere. This number can be interpreted geometrically as the number of cones or pyramids in one sphere and it is inversely proportional to the solid angle of the cone α. In Figures 1a and b, such elementary cones are sketched and they show the division into an "aromatic" (dark) and an "aliphatic" (light) region for two different values of *f*. It is clear that if the length of the aliphatic region *s* is kept constant, the cone angle α decreases with increasing *f*, with the consequential increase in the number of cones per sphere and hence an increase in sphere volume (Figures 1d, e). A simple geometrical relationship between *f* and the cell volume can therefore be found as follows. If a supramolecular dendrimer with a volume $V = a^3/8$ is assumed to be a sphere of radius *R* (Figure 1c), the "aromatic" region forms an inner sphere of radius *r* and volume *v*, with $R - r = s$ and $v/V = (r/R)^3 = f$. If *s* is a constant, then Equation (2) applies.

$$s = R - r = \left(\frac{3}{4\pi}\right)^{1/3}(V^{1/3} - v^{1/3}) = \left(\frac{3}{4\pi}\frac{a^3}{8}\right)^{1/3}(1 - f^{1/3})$$
$$\therefore \frac{a}{2}\left(\frac{3}{4\pi}\right)^{1/3} = s(1 - f^{1/3})^{-1} \quad (2)$$

In Figure 4, the experimental values $(a/2)(3/4\pi)^{1/3}$ are plotted against $(1 - f^{1/3})^{-1}$. The slope of the least squares line through the origin gives *s* as 0.97 nm. This average length of a dodecyl chain in the $Pm\bar{3}n$ phase should be compared with the extended chain length of 1.62 nm (measured from the centre

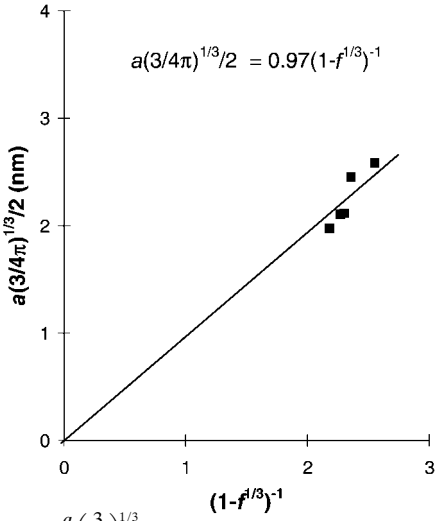

Figure 4. Plot of $\frac{a}{2}\left(\frac{3}{4\pi}\right)^{1/3}$ versus $s(1 - f^{1/3})^{-1}$ for 3,4,5-12G_1-COONa, 3,4,5-12G_1-COOCs, $(3,4,5)^2$-12G_2-COOH, $(3,4,5)^3$-12G_3-COOH and $(3,4,5)^2$-12G_2-CO$(OCH_2CH_2)_3$OH. The line represents the best fit to Equation (2).

of the O-C bond in $O(CH_2)_{12}H$ and it includes the van der Waals radius of the terminal hydrogen). A higher than equilibrium concentration of nonplanar rotamers is required for chain shortening of this magnitude and hence a considerable degree of interdigitation must exist between chains from neighbouring spheres.

In the bottom part of Table 2, data are listed for the $Pm\bar{3}n$ phase of three cesium salts with different chain lengths: 3,4,5-*n*G_1-COOCs, $n = 12$, 14 and 16. Measurements were made at the same temperature. In contrast to the comparisons above, where the different compounds all had the same terminal chains, here the increase in unit cell volume with increasing *n* can be accounted for purely by the increase in the aliphatic part of the molecular volume. The number of molecules per unit cell and hence per sphere remains constant within experimental error. Also, *f* decreases with increasing *n*, while the cone angle α remains the same. Nevertheless, the average radial length of the alkyl group increases by less than 0.2 nm as dodecyl chains are extended to hexadecyl. By comparison, the difference between extended chain lengths is 0.5 nm. The observed behaviour is not unexpected since *R* (Figure 1c) should increase approximately as $n^{1/3}$. An increase in the chain length therefore leads to an increase in average conformational disorder in the cubic phase. A similar argument applies also to the columnar phase,[6] with a less pronounced effect on conformational disorder.

Thermally induced column–sphere transition and negative thermal expansion of the lattice: Crystals of carboxylate salts 3,4,5-*n*G_1-COOM do not melt directly into the cubic liquid crystal phase but, on heating, pass first through the hexagonal

0947-6539/00/0607-1262 $ 17.50+.50/0 *Chem. Eur. J.* **2000**, *6*, No. 7

columnar phase comprised of cylindrical self-assemblies with cations clustered around the column axis. Columnar organisation of the salts is consistent with the now well-established principle that these monodendritic molecules fit into a *flat* slice-shaped volume, capable of assembly into infinite columns.[2, 3] The transition into the $Pm\bar{3}n$ cubic phase takes place in most studied salts at a higher temperature. This phase behaviour is illustrated in Figure 5, which shows a series of small-angle X-ray diffractograms of 3,4,5-16G_1-COOCs recorded during heating from the hexagonal to the $Pm\bar{3}n$ cubic phase. The columnar–cubic transition is thermoreversible.

An important clue for the understanding of this phase transition in 3,4,5-*n*G_1-COOM salts is the very pronounced temperature dependence of the hexagonal columnar lattice parameter; this can be seen in Figure 5 as a large continuous shift in the position of columnar reflections. As the temperature increases, the lattice parameter *a* decreases, that is, the columns become thinner. We interpret this reduction in column width as a decrease in the number of molecules per column cross section. In other words, as the temperature increases, redundant molecules leave their columns and assemble to constitute new columns, which lock into the existing lattice.

The suggestion that molecules are shed by their columns as the temperature increases is strongly supported by the fact that the unit cell parameter of the cubic lattice also decreases with increasing temperature. While in the columnar case an alternative explanation could be proposed, whereby columns compensate for their lateral shrinkage by extending longitudinally, rejection of surplus molecules is the only mechanism available for reducing the size of spheres in the cubic lattice, since shrinkage is isotropic. In Figure 6, we compare the temperature dependencies of unit cell parameters for both the two-dimensional hexagonal columnar and the three-dimensional cubic lattices for the three cesium salts 3,4,5-*n*G_1-COOCs with different chain lengths, that is, with $n = 14$, 16 and 18. Thermal contraction is observed for both columnar and cubic lattices for all three salts. Between its lower and upper temperature limits of existence, the columnar lattice of 3,4,5-16G_1-COOCs contracts by 10% linearly, or 20% in unit cell area. This means that there is a net decrease by one fifth in the number of 3,4,5-16G_1-COOCs molecules per column. Here we neglect the change in molar volume and assume constant intermolecular separation along the column axis. In the case of the cubic phase of 3,4,5-16G_1-COOCs, lattice shrinkage is even more striking with one fifth of the molecules cast off by the spheres (20% volume shrinkage) within a temperature range of only 30 °C.

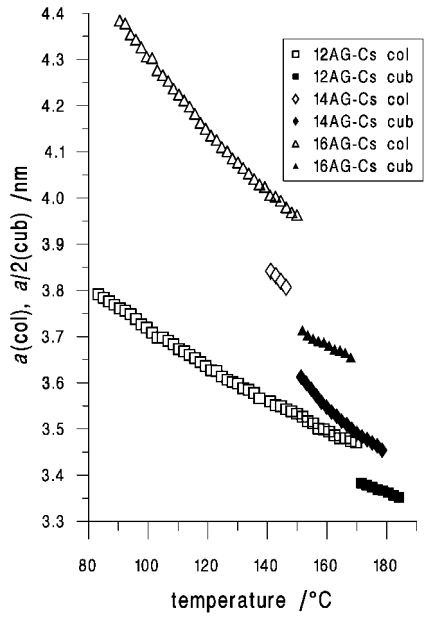

Figure 6. Temperature dependencies of the unit cell parameter *a* for the two-dimensional hexagonal columnar lattice (empty symbols) and of *a*/2 for the three-dimensional cubic lattice (shaded symbols) for cesium salts 3,4,5-12G_1-COOCs (□), 3,4,5-14G_1-COOCs (◇) and 3,4,5-16G_1-COOCs (△).

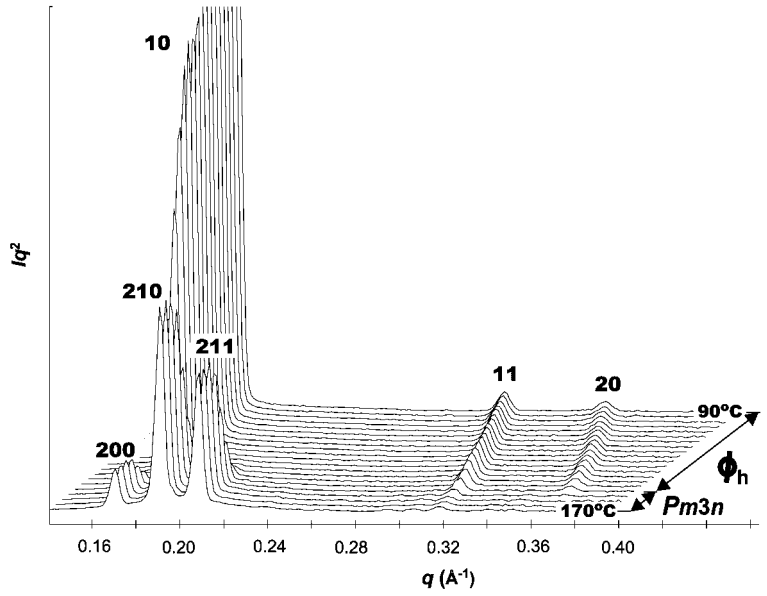

Figure 5. Series of small-angle powder diffractograms of 3,4,5-16G_1-COOCs recorded as a function of temperature. Heating rate is 5 °C min^{-1}. *hk* and *hkl* indices for the columnar and cubic diffraction peaks are marked.

The above results of course do not imply macroscopic shrinkage. In fact, a modest bulk thermal expansion is most likely. The stated estimates of the fraction of expelled molecules would have been somewhat higher had a correction for macroscopic expansion been made.

We propose that the reason that fewer molecules are retained by a spherical aggregate or a column at higher temperatures is increased conformational disorder of the alkyl chains. As the temperature increases, a higher proportion of chains are bent as a result of the

increasing population of *gauche* conformers. This means that, on average, the chains shrink longitudinally and expand laterally and thus the molecular taper angle, α, is increased. Above a critical value of α, the transition from columnar to spherical aggregates takes place. Figure 7 illustrates schematically three stages of the self-assembly of 3,4,5-nG$_1$-COOM salts, with temperature and α increasing from Figure 7a through to 7c. The cylindrical and spherical cores represent

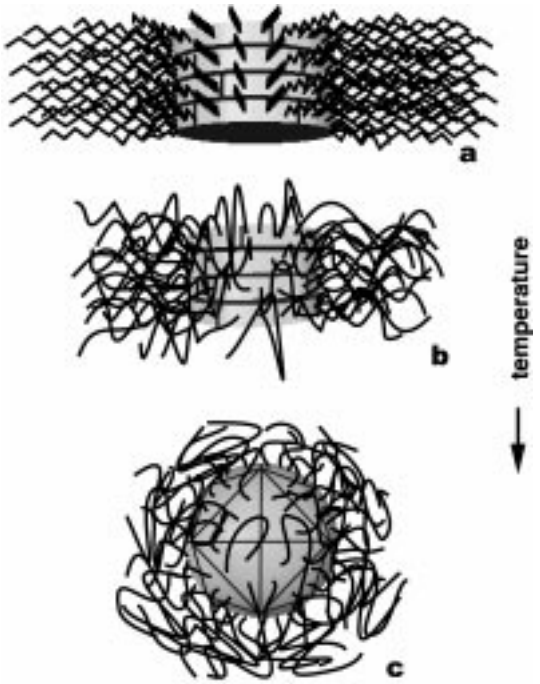

Figure 7. Schematic representation of the thermally induced shrinkage and conversion of a cylindrical into a spherical supramolecular dendrimer due to the increasing population of *gauche* conformers in the peripheral aliphatic chains.

the aromatic regions including the cations, while the tethered chains are represented by solid lines. Figures 7a and b represent a column section at a lower and a higher temperature, respectively. The column cross section in Figure 7b contains fewer segments and is thus smaller. Figure 7c shows a supramolecular sphere above the columnar–cubic transition temperature. If the temperature is increased further, the conical monodendrons become shorter and wider. Hence a decreasing number can be accommodated in a sphere and this leads to their shrinkage (Figure 1d and e).

Conclusion

In this report, we have demonstrated two principal ways of affecting the packing of tapered monodendritic molecules in supramolecular dendrimers, which self-organise to form thermotropic columnar and cubic liquid crystals: a) by changing the width of the wide (aliphatic) end, and b) by changing the volume at the apex (narrow end) of the molecules. The single most important parameter which determines the shape and size of the supramolecular dendrimer is the molecular taper angle α. In the first instance, this geometrical characteristic determines whether such molecules will self-assemble into spherical or columnar objects. Furthermore, it also controls the equilibrium size of these objects. The steric parameters of the monodendron can be controlled by both chemical design and temperature. The strong, negative thermal expansion coefficient of the cubic and columnar lattice is attributed to the excess of the increasingly tapered molecules being rejected from their parent aggregates and reassembling into new ones. An equilibrium object or aggregate size is thus maintained. Increasing taper angle is also considered to be responsible for the observed thermotropic columnar–cubic transition. We have recently observed new phases and more complex phase sequences in related systems and current investigations are revealing new relationships between molecular and mesophase structure.

Experimental Section

Materials: THF (Fisher, A.C.S. reagent) was refluxed over sodium/benzophenone ketyl and freshly distilled before use. CH_2Cl_2 (Fisher, A.C.S. reagent) was refluxed over CaH_2 and freshly distilled before use. Benzene (Fisher, A.C.S. reagent) was shaken with concentrated H_2SO_4, washed twice with water, dried over $MgSO_4$ and finally distilled over CaH_2 or sodium/benzophenone ketyl, respectively. Ethanol (EtOH), dimethylformamide (DMF) and K_2CO_3 (all Fisher, A.C.S. reagents) were used as received. $LiAlH_4$ (95 + %), NaH (80% dispersion in oil) and 3,4,5-trihydroxybenzoic acid (97%) (all from Aldrich) were used as received. The compounds 1-bromododecane (98 + %), 1-bromotetradecane (97%) and 1-bromohexadecane (98%) (all from Lancaster) were used as received. Dimethylaminopyridine (DMAP) (99%), *p*-toluene sulfonyl chloride (TsCl) (98%) and tetrabutylammonium hydrogen sulfate (TBAH) (97%) (all from Aldrich) were used as received.

General methods: ^{1}H NMR (200 MHz) and ^{13}C NMR (50 MHz) spectra were recorded on a Varian Gemini 200 spectrometer. $CDCl_3$ was used as a solvent and TMS as an internal standard unless otherwise noted. Chemical shifts are reported as δ (ppm). The purity of products was determined by a combination of techniques that include thin-layer chromatography (TLC) on silica gel plates (Kodak) with fluorescent indicator and high-pressure liquid chromatography (HPLC). HPLC measurements were carried out by using a Perkin-Elmer Series 10 high-pressure liquid chromatograph equipped with an LC100 column oven, a Nelson Analytical 900 Series integrator data station and two Perkin-Elmer PL gel columns of 5×10^2 and 1×10^4 Å. THF was used as a solvent at the oven temperature of 40 °C. Detection was by UV absorbance at 254 nm. Weight average (M_w) and number average (M_n) molecular weights were determined with the same instrument and a calibration plot constructed from polystyrene standards. Thermal transitions of samples that were freeze-dried from benzene were measured on a Perkin Elmer DSC7 differential scanning calorimeter (DSC). In all cases, the heating and cooling rates were 10 °C min^{-1} unless otherwise noted. First-order transition temperatures were reported as the maxima and minima of their endothermic and exothermic peaks. Glass-transition temperatures (T_g) were read at the point half way through the change in heat capacity. Indium and zinc were used as calibration standards. An Olympus BX40 optical) polarised microscope (100x magnification) equipped with a Mettler FP82 hot stage and a Mettler FP80 central processor was used to verify thermal transitions and characterise anisotropic textures.

In-house X-ray diffraction experiments were performed using an Image Plate area detector (MAR Research) with a graphite-monochromatised pinhole-collimated $Cu_{K\alpha}$ beam and a helium tent. Experiments were also performed at several small-angle stations of the Synchotron Radiation Source at Daresbury (UK). A double-focused beam and a quadrant detector were used. In both cases, the sample was held in a capillary within a custom-built temperature cell controlled to within ± 0.1 °C. Capillaries of the dried carboxylate salts were sealed under nitrogen. Densities, ρ, were determined by flotation in glycerol/H_2O or glycerol/MeOH. Molecular

0947-6539/00/0607-1264 $ 17.50+.50/0 *Chem. Eur. J.* **2000**, *6*, No. 7

modelling was done on a Silicon Graphics workstation using Macromodel. The analysis of the hexagonal columnar[3c] and $Pm\bar{3}n$ cubic lattices[4a] by X-ray diffraction was carried out as described in previous publications.

Synthesis: Compounds 3,4,5-nG$_1$-COOH with $n = 12$,[6, 12] 14[6] and 16[6] and (3,4,5)^i-12G$_i$-COOH,[4a] with $i = 2$, 3 and 4 were synthesised as reported previously.

General procedure for the synthesis of 3,4,5-nG$_1$-COOM, in which M = Na, Cs: In a 125 mL round-bottom flask equipped with a magnetic stirrer and condenser, 3,4,5-nG$_1$-COOCH$_3$ (0.005 mol) was dissolved in ethanol (80 mL, 90 %) at reflux temperature. Subsequently, alkaline hydroxide (MOH) (0.025 mol) was added and the mixture was stirred under reflux for 8 h. The reaction mixture was cooled to 20 °C and the crystalline product was filtered under vacuum. The resulting salt was recrystallised four times from ethanol (90 %) and dried under vacuum at 20 °C.

Na[3,4,5-tris(n-dodecane-1-yloxy)benzoate] (3,4,5-12G$_1$-COONa): Starting from 3,4,5-12G$_1$-COOCH$_3$ (3.44 g, 0.005 mol) and NaOH (1 g, 0.025 mol), 3,4,5-12G$_1$-COONa (2.43 g, yield 71.2 %) was obtained. Purity (HPLC) 99 + %. ^{1}H NMR (200 MHz, CDCl$_3$, TMS): $\delta = 0.89$ (t, $J = 6.2$ Hz, 9H; CH$_3$), 1.1 – 1.7 (overlapped, 60H; CH$_3$(CH_2)$_9$), 3.65 (m, 4H; 3,5-CH_2OPh), 3.79 (t, 2H; 4-CH_2OPh), 6.9 (s, 2H; Ar); ^{13}C NMR (50 MHz, CDCl$_3$, TMS): $\delta = 14.2$ (CH$_3$), 22.7 (CH$_3$CH_2), 25.8 (CH_2CH$_2$OPh), 28.9 – 30.1 (CH$_2$), 31.9 (CH$_3$CH$_2$CH_2), 69.5 (CH_2OPh), 108.4 (2,6-Ar), 131.5 (1-Ar), 135.2 (5-Ar), 154.1 (3,5-Ar), 176.4 (COO$^-$).

Cs[3,4,5-tris(n-dodecane-1-yloxy)benzoate] (3,4,5-12G$_1$-COOCs): Starting from 3,4,5-12G$_1$-COOCH$_3$ (3.44 g, 0.005 mol) and CsOH (3.75 g, 0.025 mol), 3,4,5-12G$_1$-COOCs (2.98 g, yield 73.9 %) was obtained. Purity (HPLC) 99 + %. ^{1}H NMR (200 MHz, CDCl$_3$, TMS): $\delta = 0.89$ (t, $J = 6.4$ Hz, 9H; CH$_3$), 1.2 – 1.8 (overlapped, 60H; CH$_3$(CH_2)$_9$), 3.64 (m, 4H; 3,5-CH_2OPh), 3.78 (t, 2H; 4-CH_2OPh), 6.92 (s, 2H; Ar); ^{13}C NMR (50 MHz, CDCl$_3$, TMS): $\delta = 14.2$ (CH$_3$), 22.6 (CH$_3$CH_2), 25.6 (CH_2CH$_2$OPh), 28.9 – 30.0 (CH$_2$), 31.8 (CH$_3$CH$_2$CH_2), 69.4 (CH_2OPh), 108.3 (2,6-Ar), 131.9 (1-Ar), 135.0 (5-Ar), 154.0 (3,5-Ar), 176.8 (COO$^-$).

Cs[3,4,5-tris(n-tetradecane-1-yloxy)benzoate] (3,4,5-14G$_1$-COOCs): Starting from 3,4,5-14G$_1$-COOCH$_3$ (3.86 g, 0.005 mol) and CsOH (3.75 g, 0.025 mol), 3,4,5-14G$_1$-COOCs (3.33 g, yield 83.5 %) was obtained. Purity (HPLC) 99 + %. ^{1}H NMR (200 MHz, CDCl$_3$, TMS): $\delta = 0.88$ (t, $J = 6.5$ Hz, 9H; CH$_3$), 1.2 – 1.7 (overlapped, 66H; CH$_3$(CH_2)$_{11}$), 3.62 (m, 4H; 3,5-CH_2OPh), 3.76 (t, 2H; 4-CH_2OPh), 6.90 (s, 2H; Ar); ^{13}C NMR (50 MHz, CDCl$_3$, TMS): $\delta = 14.1$ (CH$_3$), 22.5 (CH$_3$CH_2), 25.5 (CH_2CH$_2$OPh), 28.8 – 30.4 (CH$_2$), 31.6 (CH$_3$CH$_2$CH_2), 69.6 (CH_2OPh), 108.5 (2,6-Ar), 131.8 (1-Ar), 135.1 (5-Ar), 154.2 (3,5-Ar), 176.5 (COO$^-$).

Cs[3,4,5-tris(n-hexadecane-1-yloxy)benzoate] (3,4,5-16G$_1$-COOCs): Starting from 3,4,5-16G$_1$-COOCH$_3$ (4.28 g, 0.005 mol) and CsOH (3.75 g, 0.025 mol), 3,4,5-16G$_1$-COOCs (3.8 g, yield 78.1 %) was obtained. Purity (HPLC) 99 + %. ^{1}H NMR (200 MHz, CDCl$_3$, TMS): $\delta = 0.89$ (t, $J = 6.6$ Hz, 9H; CH$_3$), 1.1 – 1.8 (overlapped, 78H; CH$_3$(CH_2)$_{13}$), 3.60 (m, 4H; 3,5-CH_2OPh), 3.73 (t, 2H; 4-CH_2OPh), 6.92 (s, 2H; Ar); ^{13}C NMR (50 MHz, CDCl$_3$, TMS): $\delta = 14.1$ (CH$_3$); 22.4 (CH$_3$CH_2), 25.3 (CH_2CH$_2$OPh), 28.7 – 30.6 (CH$_2$), 31.5 (CH$_3$CH$_2$CH_2), 69.7 (CH_2OPh), 108.6 (2,6-Ar), 131.5 (1-Ar), 135.4 (5-Ar), 154.3 (3,5-Ar), 176.8 (COO$^-$).

Triethyleneglycol[3,4,5-tris{3′,4′,5′-tris(n-dodecane-1-yloxy)benzyloxy} benzoate] [(3,4,5)^2-12G$_2$-CO(OCH$_2$CH$_2$)$_3$OH]: The compounds (3,4,5)^2-12G$_2$-COOH[4] (4.60 g, 2.2 mmol), triethyleneglycol (4.0 g, 0.05 mol), TBAH (0.15 g, 0.45 mmol), DMAP (0.15 g, 1.23 mmol) and K_2CO_3 (1.5 g, 10.8 mmol) in THF (50 mL) were added to a round-bottomed flask. The mixture was stirred at 45 °C for 16 h. The reaction was cooled at 20 °C, poured into ice water, acidified with dilute HCl and the precipitate was filtered. The product was purified by repeated precipitations from solution in THF into water and finally by column chromatography (silica gel, CHCl$_3$) to obtain a white solid (2.42 g, yield 50 %). Purity (HPLC) 99 %. ^{1}H NMR (200 MHz, CDCl$_3$, TMS): $\delta = 0.89$ (t, 27H; CH$_3$), 1.24 (overlapped, 162H; (CH$_2$)$_9$), 1.76 (overlapped, 18H; CH_2CH$_2$OPh), 3.62 (t, 2H; CH_2OH), 3.68 (s, 6H; OCH_2CH_2O), 3.82 (t, 2H; CH_2CH$_2$O$_2$C), 3.92 (overlapped, 18H; CH_2OPh), 4.47 (t, 2H; CH_2O$_2$C), 5.04 (s, 6H; PhCH_2OPhCO$_2$), 6.58 (s, 2H; C$_6H_2$CH$_2$O), 6.62 (s, 4H; C$_6H_2$CH$_2$O), 7.42 (s, 2H; C$_6H_2$CO$_2$).

Acknowledgements

We thank the Engineering and Physical Science Research Council, the National Science Foundation (DMR-9708581) and ARO-MURI for financial support. We acknowledge Dr. B.U. Komanschek of the Daresbury Laboratory (UK) for help with the synchrotron experiments and Professor S.Z.D. Cheng of the University of Akron (USA) for the density measurements.

[1] S. Chandrasekhar in *Handbook of Liquid Crystals*, *Vol. 2B* (Eds.: D. Demus, J. Goodby, G. W. Gray, H.-W. Spiess, V. Vill), Wiley-VCH, Weinheim, **1998**, p. 749.

[2] a) J. Malthête, A. Collet, A. M. Levelut, *Liq. Cryst.* **1989**, *5*, 123; b) J. Malthête, P. Davidson, *Bull. Soc. Chim. Fr.* **1994**, *131*, 812.

[3] a) M.-J. Bienne, J. Gabard, J.-M. Lehn, I. Stibor, *J. Chem. Soc. Chem. Commun.* **1989**, 1868; b) V. Percec, G. Johansson, J. Heck, G. Ungar, S. V. Batty, *J. Chem. Soc. Perkin Trans. 1* **1993**, 1411; c) V. Percec, J. Heck, D. Tomazos, F. Falkenberg, H. Blackwell, G. Ungar, *J. Chem. Soc. Perkin Trans. 1* **1993**, 2799; d) V. Percec, J. A. Heck, D. Tomazos, G. Ungar, *J. Chem. Soc. Perkin Trans. 2* **1993**, 2381; e) V. Percec, D. Tomazos, J. Heck, H. Blackwell, G. Ungar, *J. Chem. Soc. Perkin Trans. 2* **1994**, 31; f) G. Johansson, V. Percec, G. Ungar, D. Abramic, *J. Chem. Soc. Perkin Trans. 1* **1994**, 447; g) V. Percec, G. Johansson, G. Ungar, J.-P. Zhou, *J. Am. Chem. Soc.* **1996**, *118*, 9855; h) V. Percec, W.-D. Cho, P. E. Mosier, G. Ungar, D. J. P. Yeardley, *J. Am. Chem. Soc.* **1998**, *120*, 11061; i) J. L. M. van Nunen, B. F. B. Folmer, R. J. M. Nolte, *J. Am. Chem. Soc.* **1997**, *119*, 283; j) M. Suarez, J.-M. Lehn, S. C. Zimmerman, A. Skoulios, B. Heinrich, *J. Am. Chem. Soc.* **1998**, *120*, 9526; k) G. Lattermann, G. Staufer, G. Brezinski, *Liq. Cryst.* **1991**, *10*, 169; l) U. Beginn, G. Lattermann, *Liq. Cryst.* **1994**, *241*, 215; m) S. D. Hudson, H.-T. Jung, V. Percec, W.-D. Cho, G. Johansson, G. Ungar, V. S. K. Balagurusamy, *Science* **1997**, *278*, 449; n) H. Zheng, T. M. Swager, *J. Am. Chem. Soc.* **1994**, *116*, 771; for two brief reviews see: o) V. Percec, G. Johansson, D. Schlueter, J. C. Ronda, G. Ungar, G. *Macromol. Symp.* **1996**, *101*, 43; p) C. M. Paleos, D. Tsiourvas, *Angew. Chem.* **1995**, *107*, 1839; *Angew. Chem. Int. Ed. Engl.* **1995**, *34*, 1696.

[4] a) V. S. K. Balagurusamy, G. Ungar, V. Percec, G. Johansson, *J. Am. Chem. Soc.* **1997**, *119*, 1539; b) V. Percec, C.-H. Ahn, G. Ungar, D. J. P. Yeardley, M. Moller, S. S. Sheiko, *Nature* **1998**, *391*, 161; c) V. Percec, C.-H. Ahn, W.-D. Cho, A. M. Jamieson, J. Kim, T. Leman, M. Schmidt, M. Gerle, M. Moller, S. A. Prokhorova, S. S. Sheiko, S. Z. D. Cheng, A. Zhang, G. Ungar, D. J. P. Yeardley, *J. Am. Chem. Soc.* **1998**, *120*, 8619.

[5] a) A. Klug, *Angew. Chem.* **1983**, *95*, 579; *Angew. Chem. Int. Ed. Engl.* **1983**, *22*, 565; b) A. J. Levine, *Viruses*, Freeman, New York, **1992**.

[6] G. Ungar, D. Abramic, V. Percec, J. Heck, *Liq. Cryst.* **1996**, *21*, 73.

[7] a) V. Percec, M. Lee, J. Heck, H. E. Blackwell, G. Ungar, A. Alvarez-Castillo, *J. Mater. Chem.* **1992**, *2*, 931; b) V. Percec, J. Heck, M. Lee, G. Ungar, A. Alvarez-Castillo, *J. Mater. Chem.* **1992**, *2*, 1033; c) G. Johansson, V. Percec, G. Ungar, J.-P. Zhou, *Macromolecules*, **1996**, *29*, 646; d) V. Percec, D. Schlueter, J. C. Ronda, G. Johansson, G. Ungar, J.-P. Zhou, *Macromolecules*, **1996**, *29*, 1464; e) V. Percec, D. Schlueter, G. Ungar, S. Z. D. Cheng, A. Zhang, *Macromolecules*, **1998**, *31*, 1745; f) Z. Bao, K. R. Amundson, A. J. Lovinger, *Macromolecules*, **1998**, *31*, 8647; g) U. Stebani, G. Latermann, *Macromol. Rep.* **1995**, *A32*, 385; h) U. Stebani, G. Latermann, R. Festag, M. Wittenberg, J. H. Wendorff, *J. Mater. Chem.* **1995**, *5*, 2247; i) H. Fisher, T. Plesnivy, H. Ringsdorf, M. Seitz, *J. Chem. Soc. Chem. Commun.* **1995**, 1615; j) M. J. Seitz, T. Plesnivy, K. Schimmosek, M. Edelman, H. Ringsdorf, H. Fisher, H. Uyama, S. Kobayashi, *Macromolecules* **1996**, *29*, 6560; k) Y. K. Kwon, S. Chvalun, J. Blackwell, V. Percec, J. Heck, *Macromolecules* **1995**, *28*, 1552; l) Y. K. Kwon, S. Chvalun, A. I. Schneider, J. Blackwell, V. Percec, J. Heck, *Macromolecules* **1994**, *27*, 6129; m) S. A. Prokhorova, S. S. Sheiko, M. Moller, C.-H. Ahn, V. Percec, *Macromol. Rapid Commun.* **1998**, *19*, 359.

[8] G. Ungar, S. V. Batty, V. Percec, J. Heck, G. Johansson, *Adv. Mater. Opt. Elec.* **1994**, *4*, 303.

[9] J. Charvolin, J. F. Sadoc, *J. Phys.* (*Paris*) **1988**, *49*, 521.

[10] a) K. Fontell, K. K. Fox, E. Hansson, *Mol. Cryst. Liq. Cryst. Lett. Sect.* **1985**, *1*, 9; b) R. Vargas, P. Mariani, A. Gulik, V. Luzzati, *J. Mol. Biol.*

1992, *225*, 137; c) V. Luzzati, R. Vargas, P. Mariani, A. Gulik, H. Delacroix, *J. Mol. Biol.* **1993**, *229*, 540.

[11] This is calculated from the known volume of an aggregate (sphere), taken as one eighth of the unit cell volume (Table 2). Macroscopic density was measured for annealed $(3,4,5)^2$-12G_2-X as 0.99 g cm^{-3}. Densities of other compounds were calculated from their molecular mass and van der Waals volume; this assumes the same packing efficiency of 0.67 as derived for $(3,4,5)^2$-12G_2-X.

[12] V. Percec, C.-H. Ahn, T. K. Bera, G. Ungar, D. J. P. Yeardley, *Chem. Eur. J.* **1999**, *5*, 1070.

Received: June 1, 1999 [F1829]

  0947-6539/00/0607-1266 $ 17.50+.50/0 *Chem. Eur. J.* **2000**, *6*, No. 7